Optics Letters

60 dB high-extinction auto-configured Mach–Zehnder interferometer

C. M. Wilkes,[1,*] X. Qiang,[1] J. Wang,[1] R. Santagati,[1] S. Paesani,[1] X. Zhou,[2] D. A. B. Miller,[3] G. D. Marshall,[1] M. G. Thompson,[1] and J. L. O'Brien[1,3]

[1]Quantum Engineering Technology Labs, H. H. Wills Physics Laboratory and Department of Electrical and Electronic Engineering, University of Bristol, BS8 1FD, UK
[2]State Key Laboratory of Optoelectronic Materials and Technologies and School of Physics and Engineering, Sun Yat-sen University, Guangzhou 510275, China
[3]Ginzton Laboratory, Spilker Building, Stanford University, 348 Via Pueblo Mall, Stanford, California 94305-4088, USA
*Corresponding author: callum.wilkes@bristol.ac.uk

Received 1 September 2016; revised 12 October 2016; accepted 13 October 2016; posted 20 October 2016 (Doc. ID 275023); published 11 November 2016

Imperfections in integrated photonics manufacturing have a detrimental effect on the maximal achievable visibility in interferometric architectures. These limits have profound implications for further technological developments in photonics and in particular for quantum photonic technologies. Active optimization approaches, together with reconfigurable photonics, have been proposed as a solution to overcome this. In this Letter, we demonstrate an ultrahigh (>60 dB) extinction ratio in a silicon photonic device consisting of cascaded Mach–Zehnder interferometers, in which additional interferometers function as variable beamsplitters. The imperfections of fabricated beamsplitters are compensated using an automated progressive optimization algorithm with no requirement for precalibration. This work shows the possibility of integrating and accurately controlling linear-optical components for large-scale quantum information processing and other applications.

OCIS codes: (120.3180) Interferometry; (130.3120) Integrated optics devices; (230.7370) Waveguides; (250.5300) Photonic integrated circuits; (270.0270) Quantum optics; (270.5585) Quantum information and processing.

http://dx.doi.org/10.1364/OL.41.005318

Photonic technology has been advancing rapidly, especially with platforms such as silicon photonics [1], with many potential applications in classical interconnects, communications, and sensing [2], where it offers solutions to increasing problems of interconnect density and energy inside machines [3,4], complements the processing abilities of electronics [5], and provides novel possibilities such as mode-division multiplexing [2] at long distances. Also, photonics is considered a promising physical implementation for quantum information technologies, including quantum communication [6,7], metrology [8,9], and computation [10–12]. This is owing to the photon's properties of long coherence time and ease of manipulation [13–15]. Many of these photonic technologies require precise interference of beams, for example in Mach–Zehnder interferometers (MZIs) consisting of a phase-shifter and two outer beamsplitters (BSs). A key difficulty is, however, that component fabrication is imprecise.

As the integration density of photonic components increases, high-performance MZIs will become extremely valuable because any operation error of a single MZI will propagate along the circuit and accumulate exponentially. This is especially true for fault-tolerant linear optical quantum computing [16–18]. The quality of a high-performance MZI is typically quantitatively described by its extinction ratio. The extinction ratio, in the presence of indistinguishable photons, is a measure of how well one can distinguish between orthogonal computational basis states, and it is fundamentally determined by the splitting ratios of the BSs used in the MZIs themselves [13,14]. Because of fabrication imperfections, integrated BSs usually have different splitting ratios to the desired ones—sometimes quite far away from 50:50 [19,20]. Fortunately, the technique demonstrated in this Letter compensates for such imperfections, making photonic devices tolerant to these faults.

A common practice in optics is to use additional MZIs to act as reconfigurable variable BSs (VBSs) [21,22], creating characterization difficulties if all passive components are replaced by these. A possible solution is presented by the combined use of these active components together with automated optimization techniques [23,24]. The optimal VBS configuration is easily found by our auto-configuration algorithm. In this way, it is possible to compensate for fabrication imperfections to achieve high-visibility interference in MZIs. Previous compensation

schemes in integrated silicon [20] (by a variable MZI) and integrated lithium niobate [25] photonics (with active trimming) use just one tunable BS that is optimized iteratively. Because of this they are still subject to fabrication imperfections, thereby limiting their performance. With a linear increase in optical resources, we can fully overcome imperfect fabrication. The scheme demonstrated in this Letter works very well for general large-scale optical circuits, with the VBS MZIs as functional building blocks across the circuit.

Here we present, to the best of our knowledge, the first experimental demonstration of a near-perfect MZI on a silicon photonic chip by implementing the adaptive self-optimized approach proposed in Ref. [24]. This method consists of using two additional MZIs acting as VBSs and finding their optimal configuration, thereby circumventing the requirements for perfectly fabricated BSs. This progressive approach allows automatic optimization of the splitting ratios of two VBSs to 50:50—without any prior calibration—and results in a high-extinction-ratio MZI. Using a silicon photonic device, we measured 60.5 dB extinction in the interferometric fringes, corresponding to an increase of 29.6 dB with respect to the nonoptimized case. This work represents the latest in achievable extinction for interference and an approach for the realization of ultrahigh fidelity operations for future fault-tolerant linear optical quantum computing [18].

Figure 1 shows the schematic of the MZI consisting of seven components, each with their own parameter: three thermo-optical phase-shifters (H_L, H_R, and H_{MZI}) with phases that we scan over and four passive BSs with fixed splitting ratios that are not of direct interest, as long as they fall within a range of 85:15–15:85 [24]. The phase-shifters are resistive heating elements, and they induce a local change in the refractive index of the waveguide core by temperature variation. This allows us to optimize and control the MZI by applying electrical voltage onto each phase-shifter. To achieve an optimized MZI, we want to find the voltage settings for the outer phase-shifters, H_L and H_R, that construct the VBSs to be BSs of 50:50 splitting ratio. Once this has been determined, the H_L and H_R can be set to the constant phase and the central H_{MZI} varied as a usual phase-shifter in a MZI.

To find the optimum voltage settings for H_L and H_R we use an algorithm that enables us to set both VBS_L and VBS_R to 50:50 reflectivity, without pre-calibrating any component and only by simply minimizing or maximizing optical power in one output port [24]. Considering the optical power output at port 3, and rephrasing the reflectivities (i.e., splitting ratios) in their offset from the ideal 50:50 case ($\delta R_i = R_i - 0.5$),

$$P^{(3)} = \frac{1}{2} + 2\left\{\delta R_L \delta R_R - \sqrt{\left[\frac{1}{4} - \delta R_L^2\right]\left[\frac{1}{4} - \delta R_R^2\right]}\cos\theta\right\}, \tag{1}$$

where R_i is the fabricated reflectivity of each VBS, θ is the phase of H_{MZI}, and $P^{(3)}$ is the normalized measured optical power at port 3. The maximum and minimum power, respectively, correspond to $\theta = \pi$ and $\theta = 0$, with the cosine of θ therefore giving a sign change in the last term of Eq. (1). At these settings of the H_{MZI} phase we determine the optimal voltages for H_L and H_R. The problem of configuring the VBS is thus reduced to a two-dimensional optimization problem over the reflectivities, R_L and R_R, of the two VBSs. The convergence point of the algorithm [24] is exactly at the point where both reflectivities are 0.5—that is, δR_L and δR_R are zero.

We use the algorithm of [24], though we have to extend it here because we do not have reliable prior knowledge of exactly which range of phase-shifter voltages corresponds to monotonic increase or decrease of the splitting ratios of VBS_L and VBS_R; for each such BS, that monotonic range will occur only over a specific range of size π somewhere in a total 2π range of phase shifts. So, we end up exploring the whole 2π range for both BSs to minimize or maximize power. We do this for the first pass of the algorithm; with subsequent passes we adapt the scan range to a smaller one centered on previously obtained voltage values. We start with all voltages set to zero. Hence our extended algorithm becomes:

1. Scan over the 2π voltage range of H_{MZI} to obtain the voltage for the minimum power at output port 3, $P^{(3)}_{\mathrm{min}}$.
2. Scan H_L and H_R over their voltage ranges in both equal and identical directions to find minimum power, $(\delta V_{H_L}, \delta V_{H_R}) \ni \{(+,+),(-,-)\}$, where + means up, and – means down.
3. Scan over the 2π voltage range of H_{MZI} to obtain the voltage for the maximum power at output port 3, $P^{(3)}_{\mathrm{max}}$.
4. Scan H_L and H_R over their voltage ranges in all four equal and identical, and equal and opposite directions to find the maximum optical power, $(\delta V_{H_L}, \delta V_{H_R}) \ni \{(+,+),(+,-),(-,+),(-,-)\}$.
5. Repeat steps 1–4 until there are no further statistically significant and measurable changes in V_{H_L}, V_{H_R} settings.

Figure 2(a) depicts a typical calculated optical power response for a VBS MZI when it is subject to variation in the phase-shifter voltages, V_L and V_R. The region plots were obtained by evaluating Eq. (1) for the maximum (minimum) power case by equating them to the maximum (minimum) normalized power of 1 (0). The lines shown are contours for optical powers within a specified range of values. This threshold value is 0.995 (0.003) for the maximum (minimum) case.

The MZI device was fabricated on a standard silicon-on-insulator wafer using 248 nm photo-lithography technology. The BSs use a multi-mode interference (MMI) structure, and thermo-optical phase-shifters were formed using TiN resistive heaters. The as-fabricated MMIs possess various splitting ratios that deviate from the ideal 50:50. The chip was mounted on a thermo-electrically controlled copper plate for stable temperature maintenance. Waste heat was dumped to a large

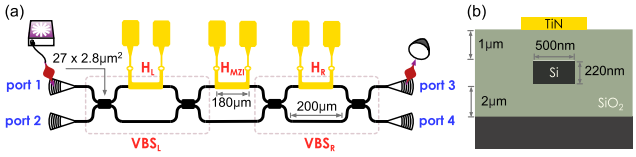

Fig. 1. (a) Self-optimized Mach–Zehnder interferometer (MZI) and experimental setup. The cascaded MZI device was fabricated in silicon photonic waveguides. It consists of three thermo-optical phase-shifters and four multi-mode interference (MMI) beamsplitters (BSs). The dimensions of the common variable BSs (VBSs), central MZI, MMIs, and phase-shifters are all the same. The H_L and H_R thermal phase-shifters, together with their adjacent BSs, form the VBSs (dashed boxes), and H_{MZI} phase-shifter offers the usual control of the MZI interference. (b) Cross-section diagram of a MZI arm with a thermo-optical phase-shifter on top.

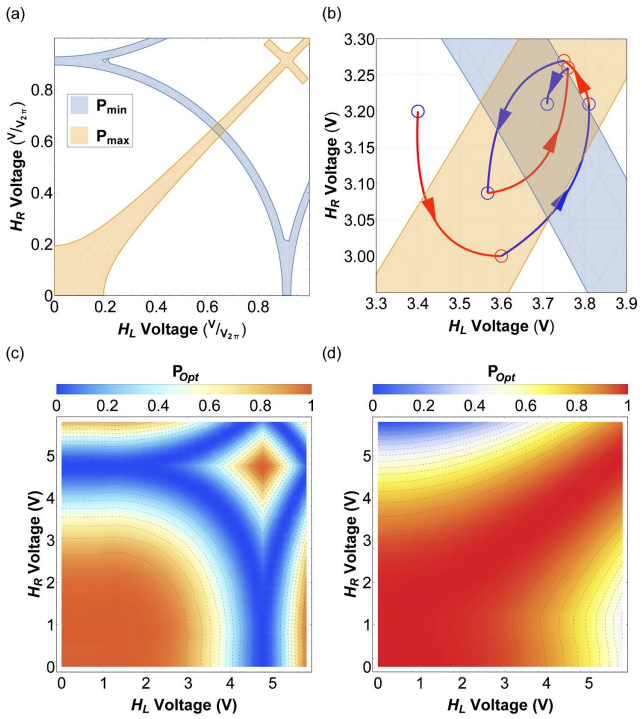

Fig. 2. (a) Simulation of the BS setup algorithm with initial MMI splitting ratios of 50.0:50.0, zero internal MZI phase differences, and zero phase-shifter phase-voltage offsets. The blue (orange) area represents the minimum (maximum) optical power $P_{\min}$ ($P_{\max}$) at port 3 with a change of V_{H_L} and V_{H_R}. The algorithm ultimately converges where the two areas intersect. Note that there are periodic solutions; the region shown is chosen within the first 2π phase voltage of both H_L and H_R. This convergence point is easier to locate as phase scales with the square of the voltage. (b) Experimental convergence of the self-optimized algorithm. Each point plotted indicates the H_L and H_R voltage settings obtained after steps 2 (blue) and 4 (red) for subsequent passes of the algorithm. (The colored arrow paths are guides for the eye, but the points are experimental results at the end of each stage of the algorithm.) Rapid convergence occurred, with the optimal point at (3.71 V,3.21 V), determining the 50:50 configuration of both VBS_L and VBS_R. (c) and (d) The fitted surfaces from experiment data for minimum and maximum optical power, confirming the expected convergence lines shown in (a).

copper heat sink. Each phase-shifter has a separate signal pin and mutually referenced ground pin, and was controlled by an individual voltage driver. Thermal crosstalk was negligible, and the device remained in a steady thermal state throughout.

Laser light at 1550.8 nm wavelength from a Tunics T100S-HP laser was coupled to the chip using grating couplers and a single-mode fiber array mounted on a piezo-controlled 6-axis translation stage. The chip remained stable through our experiments and required no active intervention to counter misalignment or aging. The grating coupler here also works as an on–chip transverse-electric (TE) polarizer [26], ensuring that all MZI components interact only with the TE-polarized light, thereby avoiding visibility degradation from an impure polarization state meeting in the MMIs. Before (after) light enters (leaves) the chip, it passes through a dense-wavelength-division multiplexer (DWDM) filter to reduce the amplified spontaneous emission noise from the laser and background signal from flat spectrum scattered light across the slab mode of the chip. Light is detected by a high-sensitivity Thorlabs S155C InGaAs power meter with a dynamic range of 80 dB. All resistive heaters are controlled by a 12-bit in-house digital-to-analog converter (DAC) electrical driver, which enables us to scan them with high accuracy.

The algorithm for finding the 50:50 VBS configuration was run on the device. The demonstration's results shown in Fig. 2(b) indicate a rapid convergence, caused by finding the region of the global extrema in the algorithm's first pass. This was achieved using the smallest voltage resolution available from the voltage driver (5 mV). The scan time to configure the MZI is ~4 hours, and this is presently limited by the slow communication speeds of our voltage drivers. In the absence of this bottleneck a scan would take ~20 min. The scan is a one-time process, due to negligible aging of the phase-shifters. Here, both VBSs were optimized as close to 50:50 allowable by both the algorithm and the equipment used. The subsequent MZI fringe measurement is a means of determining whether the BSs are optimized or not. Throughout the experiment, light was injected into port 1, and the optical power was measured only at port 3. This was important for demonstrating the capabilities of the algorithm, and that it only requires a single optical signal output to inform the voltage settings for subsequent steps.

Figures 2(c) and 2(d) are the 2D fits of experimental data over the 2π voltage space of the phase-shifters for the maximum and minimum optical power cases. These confirm the theoretical plot, Fig. 2(a). The fits are obtained with a cubic phase–voltage relationship of the phase-shifters, a relationship that has also been considered for other integrated photonic devices [13]. The cubic term encapsulates all nonohmic behavior of the phase-shifters, such as their change in resistance when subject to higher temperatures.

With the use of the self-optimized VBS_L and VBS_R we then implement the MZI. The MZI yielded an ultrahigh extinction ratio of 60.5 dB (Fig. 3). For comparison, a fringe of 30.9 dB was measured for a single MZI on the same chip with two fixed MMI BSs, corresponding to BSs with a 48.4:51.6 splitting ratio. Here it is assumed that both MMIs possess the same splitting ratio and that there is no loss imbalance in the two arms (which is probably the case). This illustrates the significant improvement offered—29.6 dB in this case—by compensating for fabrication imperfections. Moreover, our demonstration is a 10.1 dB increase from the previous reported result in silicon using an active device consisting of only one VBS [20]. By design, our MMIs have a relatively flat wavelength response of 3 ± 0.4 dB over a bandwidth of 30 nm [27], and we expect our algorithm to obtain optimized VBSs over at least this spectrum.

The measured extinction ratio of 60.5 dB is at the limit of the DAC resolution of our voltage drivers. In the deepest region of the fringe a small change in the applied voltage can induce a sharp change in the optical power. The sinusoidal nature of the phase control relationship works against us for achieving 50:50 splitting ratio VBSs because this is the point where the rate of change of splitting ratio with respect to voltage is the greatest. Increasing the number of bits in our DAC can yield a linear increase in the extinction ratio by 5–8 dB per bit (depending on the passive BS split ratios). An 18-bit DAC could theoretically yield an extinction ratio of 100 dB, when decoupled from other contributions. As a further development, we could use

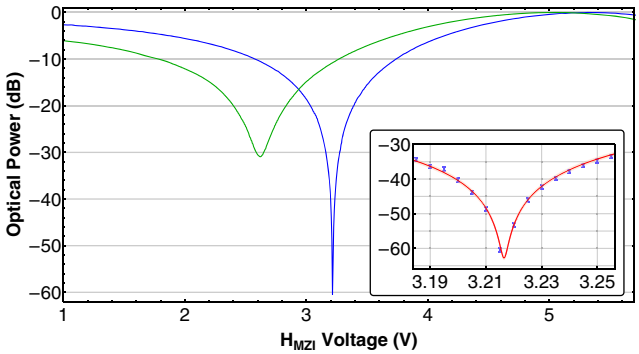

Fig. 3. High-extinction-ratio MZI interference fringe. Blue is the fringe obtained using self-optimized MZI BSs, with 60.5 dB extinction ratio. Green is the fringe obtained using a single MZI with as-fabricated BSs, with 30.9 dB extinction ratio. Both fringes were taken under the same experimental conditions. Inset shows a closeup of the fringe's dip, showing that the power readings in that region are well-behaved and are not due to any noise in the measurement apparatus. All extinction ratios were obtained from the raw data values.

VBS MZI devices where the BSs are close to the 85:15 splitting ratio allowed by the algorithm (but far enough that the statistical variations never exceed that). This would give a flatter response for the variable reflectivity, improving performance significantly with the number of bits. There is thus plenty of scope for further enhancing our MZI's performance.

We have experimentally demonstrated a one-part-in-a-million 60 dB high-extinction-ratio MZI (despite imperfect fabrication of BSs) using a self-adjustment approach and without calibrating any components (Fig. 3). The result has many potential applications in several fields, from the realization of high-quality photonics for telecommunication to the development of quantum photonic technologies. The optimized VBS MZI such as ours can be cast as a functional building block, which is repeated across a triangular array to form a Reck circuit for universal linear optics [24,28]. By virtue of the VBS MZI's improved extinction, one can access proportionately more of the total state space. Calibration of complex many-mode Reck schemes with high-extinction VBS MZIs is easier and more accurate. It is also likely to be quicker because of the reduced propagation of errors in measurements. These reasons illustrate how using the VBS MZI increases the maximum size of any meaningful and useful Reck scheme.

The realization of near-perfect BSs and MZIs is essential to reducing the cumulative error in quantum operations and thus significantly reducing overhead resources for fault-tolerant linear optical quantum computing [16–18]. The reason is that the number of error-correcting qubits scales inversely with the operation errors associated with BS imperfections [18]. Generally, this self-adjustable interferometric architecture could yield large-scale integration of linear-optical circuits for quantum information processing.

Funding. Engineering and Physical Sciences Research Council (EPSRC); Marie Curie ITN; Photonic Integrated Compound Quantum Encoding (PICQUE); Multidisciplinary University Research Initiative grants, Air Force Office of Scientific Research (AFOSR) (FA9950-12-1-0024); U.S. Army Research Office (ARO) (W911NF-14-1-0133).

Acknowledgment. The authors wish to thank J. Silverstone, L. Kling, A. Murray, and A. Laing for discussion and experimental assistance. M. G. Thompson acknowledges fellowship support from EPSRC. J. L. O'Brien. acknowledges a Royal Society Wolfson Merit Award and a Royal Academy of Engineering Chair in Emerging Technologies.

REFERENCES

1. D. Thomson, A. Zilkie, J. E. Bowers, T. Komljenovic, G. T. Reed, L. Vivien, D. Marris-Morini, E. Cassan, L. Virot, J.-M. Fédéli, J.-M. Hartmann, J. H. Schmid, D.-X. Xu, F. Boeuf, P. O'Brien, G. Z. Mashanovich, and M. Nedeljkovic, J. Opt. **18**, 073003 (2016).
2. E. Agrell, M. Karlsson, A. R. Chraplyvy, D. J. Richardson, P. M. Krummrich, P. Winzer, K. Roberts, J. K. Fischer, S. J. Savory, B. J. Eggleton, M. Secondini, F. R. Kschischang, A. Lord, J. Prat, I. Tomkos, J. E. Bowers, S. Srinivasan, M. Brandt-Pearce, and N. Gisin, J. Opt. **18**, 063002 (2016).
3. D. A. B. Miller, Proc. IEEE **97**, 1166 (2009).
4. A. V. Krishnamoorthy, H. Schwetman, X. Zheng, and R. Ho, J. Lightwave Technol. **33**, 889 (2015).
5. ITRS, "International technology roadmap for semiconductors 2.0," 2015, http://www.itrs2.net/itrs-reports.html.
6. C. Bennett and G. Brassard, in *Proceedings of IEEE International Conference on Computers, Systems and Signal Processing* (ACM, 1984), p. 8.
7. B. Korzh, C. C. W. Lim, R. Houlmann, N. Gisin, M. J. Li, D. Nolan, B. Sanguinetti, R. Thew, and H. Zbinden, Nat. Photonics **9**, 163 (2015).
8. M. J. Holland and K. Burnett, Phys. Rev. Lett. **71**, 1355 (1993).
9. J. P. Dowling, Contemp. Phys. **49**, 125 (2008).
10. E. Knill, R. Laflamme, and G. J. Milburn, Nature **409**, 46 (2001).
11. M. A. Nielsen and I. L. Chuang, *Quantum Computation and Quantum Information*, 10th ed. (Cambridge University, 2011).
12. J. L. O'Brien, A. Furusawa, and J. Vuckovic, Nat. Photonics **3**, 687 (2009).
13. P. J. Shadbolt, M. R. Verde, A. Peruzzo, A. Politi, A. Laing, M. Lobino, J. C. F. Matthews, M. G. Thompson, and J. L. O'Brien, Nat. Photonics **6**, 45 (2012).
14. J. Carolan, C. Harrold, C. Sparrow, E. Martn-López, N. J. Russell, J. W. Silverstone, P. J. Shadbolt, N. Matsuda, M. Oguma, M. Itoh, G. D. Marshall, M. G. Thompson, J. C. F. Matthews, T. Hashimoto, J. L. O'Brien, and A. Laing, Science **349**, 711 (2015).
15. J. Wang, D. Bonneau, M. Villa, J. W. Silverstone, R. Santagati, S. Miki, T. Yamashita, M. Fujiwara, M. Sasaki, H. Terai, M. G. Tanner, C. M. Natarajan, R. H. Hadfield, J. L. O'Brien, and M. G. Thompson, Optica **3**, 407 (2016).
16. R. Raussendorf and H. J. Briegel, Phys. Rev. Lett. **86**, 5188 (2001).
17. D. E. Browne and T. Rudolph, Phys. Rev. Lett. **95**, 010501 (2005).
18. T. Rudolph, "Why I am optimistic about the silicon-photonic route to quantum computing," arXiv: 1607.08535 (2016).
19. K. Suzuki, K. Tanizawa, T. Matsukawa, G. Cong, S.-H. Kim, S. Suda, M. Ohno, T. Chiba, H. Tadokoro, M. Yanagihara, Y. Igarashi, M. Masahara, S. Namiki, and H. Kawashima, Opt. Express **22**, 3887 (2014).
20. K. Suzuki, G. Cong, K. Tanizawa, S.-H. Kim, K. Ikeda, S. Namiki, and H. Kawashima, Opt. Express **23**, 9086 (2015).
21. C. K. Madsen, G. Lenz, A. J. Bruce, M. A. Cappuzzo, L. T. Gomez, and R. E. Scotti, IEEE Photon. Technol. Lett. **11**, 1623 (1999).
22. B. J. Offrein, F. Horst, G. L. Bona, R. Germann, H. W. M. Salemink, and R. Beyeler, IEEE Photon. Technol. Lett. **12**, 504 (2000).
23. D. A. B. Miller, Photon. Res. **1**, 1 (2013).
24. D. A. B. Miller, Optica **2**, 747 (2015).
25. Y. Yamaguchi, S. Nakajima, A. Kanno, T. Kawanishi, M. Izutsu, and H. Nakajima, Jpn. J. Appl. Phys. **53**, 08MB03 (2014).
26. D. Taillaert, H. Chong, P. I. Borel, L. H. Frandsen, R. M. D. L. Rue, and R. Baets, IEEE Photon. Technol. Lett. **15**, 1249 (2003).
27. H. Zhou, J. Song, C. Li, H. Zhang, and P. G. Lo, IEEE Photon. Technol. Lett. **25**, 1149 (2013).
28. M. Reck, A. Zeilinger, H. J. Bernstein, and P. Bertani, Phys. Rev. Lett. **73**, 58 (1994).